Heliyon 11 (2025) e40862

Contents lists available at ScienceDirect

Heliyon

journal homepage: www.cell.com/heliyon

Research article

Encapsulated Fe_3C boosted electrocatalytic performance for oxygen reduction reaction of N-doped carbon nanotube

Jun Dong [a,c,*], Qiqi Jiao [b,**], Hao Wang [c,d], Hong Wang [a], Yi-ke Ren [a]

[a] School of Aerospace Engineering, Xi'an Jiaotong University, Xi'an, 710049, China
[b] Shandong Provincial Hospital Affiliated to Shandong First Medical University, 324 Jingwu Road, Jinan, 250021, China
[c] China Rongtong Resources Development Group Co. Ltd., Beijing, 100081, China
[d] Liaoning Qingyang Chemical Industry Corporation, Liaoyang, 111000, China

ARTICLE INFO

Keywords:
Electrocatalysts
Oxygen reduction reaction
Fe_3C
N-doped CNT
Encapsulation structure

ABSTRACT

The shortcomings of precious metal based catalysts have limited the development of novel energies. So, developing low-cost and high performance transition metal based catalysts is one of the most feasible way to substitute the precious metal based catalysts. In all of the developed catalysts for oxygen reduction reactions (ORR), the iron-based nitrogen doped carbon nanotube (N-CNT) show great promise. In this paper, N-CNT with Fe_3C encapsulated based catalysts (Fe_3C@N-CNT) were synthesized. The encapsulation structure of Fe_3C@N-CNT was confirmed by HAADF-STEM, XANES, XPS, XRD, SEM and other methods. XANES tests show that the doped nitrogen of Fe_3C changed the length of Fe-C bond and furtherly influenced the electron transfer between encapsulated Fe_3C and outer layer N-CNT. Electrochemical tests showed that the half-wave potential and onset potential ORR of 750 °C calcined Fe_3C@N-CNT were 90 mV higher than that of 20 wt% Pt/C. The additional electric field between Fe_3C and N-CNT modulated the C-N bond of surface N-CNT and enhanced the catalytic performance for ORR. This paper reveal that constructing encapsulated additional electron providing center is an effective way to design high performance catalysts.

1. Introduction

The limited sources and high-cost of precious metal based catalysts have inhibited the development and application of novel energies. Developing non-precious metal based catalysts are highlighted by scientists and engineers in recent decades. Non-precious-metal based high cost-effective catalysts for oxygen reduction reaction (ORR) such as metal carbides, nitrides, sulfides, oxides [1], carbon based materials [2] and alloys [3] etc. have been investigated. For example, the Co-C [4], Mn-Co oxide [5], high-valent iron [6], vanadium carbide and nitride based catalysts [7,8] have been reported. It is concluded that combining with high conductivity material, introducing dopant, and construct vacancies are effective ways to improve the electrocatalytic performance for ORR of transition-metal based catalysts [9]. In all of the transition metals, the iron has the special advantages for catalyzing the synthesis of CNT. On the other hand, as the element for cementite, the iron can easily combine with carbon and nitrogen that can promote the formation of nitrogen and carbon coexisted composites. It is also reported that the iron can form single atom catalyst through the

* Corresponding author. School of Aerospace Engineering, Xi'an Jiaotong University, Xi'an, 710049, China.
** Corresponding author.
E-mail addresses: dongjun@xjtu.edu.cn (J. Dong), 934830158@qq.com (Q. Jiao).

https://doi.org/10.1016/j.heliyon.2024.e40862
Received 15 October 2024; Received in revised form 28 November 2024; Accepted 30 November 2024
Available online 3 December 2024

conjunction of nitrogen atoms. So, it can be supposed that the iron can promote the formation of nitrogen containing CNT with enough catalytic active site for ORR. The Fe-C-N based catalysts with the active site of Fe-N_4 showed the current of 33 mA/cm^2 at 0.9 V of H_2-O_2 fuel cells [10]. Edge functionalized polyphthalocyanine networks derived two-dimensional carbon supported CoN_4 based catalysts for ORR [11]. The carbon based support played the skeleton role for metal species. The nitrogen that doped to carbon support and combined with Fe/Co played the function of catalytic active center, which promoted the transition of oxygen molecular to ions. Similarly, the combination of earth-abundant transition metal oxides with carbon nanotube (CNT) led to strong synergistic interactions on adjusting the catalytic activity [12]. Compared with carbon physically supported catalysts, the in-situ derived carbon supported metal carbide with chemical combination displayed higher catalytic performance. For example, the in-situ derived TiC from CNT displayed robust catalytic characteristics for ORR in both acidic and alkaline electrolytes [13]. The co-axis structure of CNT and TiC improved the electron transfer rate between catalysts and oxygen molecular.

The high conductivity for electron and rich catalytic active centers made the nano-carbon based materials to be high performance catalysts for ORR [14]. The strong catalytic performance for ORR of N-doped graphitic materials had been confirmed [15]. The encapsulated Co/CoO made the N-doped carbon and CNT exhibited higher catalytic performance for ORR [16]. At the same time, the oxygen vacancy content, morphology and doped nitrogen combination states of carbon could be finely modulated by mixed Co-MOF and certain amounts of melamine. Synergistic effect between the glucose derived N-doped CNTs/Ni and multivalent CoSx assured the high catalytic performances for ORR [17]. Ni induced electron redistribution in carbon support enhanced the activation of adsorbed O_2 and furtherly improved the catalytic kinetics for ORR. Combination of CNT and transition metal compounds enhances the catalytic performance for ORR. Metal based species that can provide additional electrons improve the catalytic performance of carbon based materials for ORR.

Kinds of reports show that the catalytic performance for ORR can be modulated by the interaction between CNT and transition metals. The mechanism for the modulation was just explained by the synergistic effect. With the development of transition metal-carbon based catalysts, a scientific theory for the modulation should be clarified. In this paper, the in-situ synthesized N-CNT with Fe_3C encapsulated catalysts were employed to study the catalytic mechanism for ORR. The eutectic covalent carbon atoms connected the out-layer N-CNT and inner Fe_3C particles, which resulted in changes of the electron state of outer layer N-CNT. On the other hand, the different polarization state of covalent Fe-C bond of Fe_3C and C-N bond of N-CNT modulated the combining bond states of doped nitrogen and surrounding carbon atoms, which eventually made great influences on the catalytic performances for ORR. Results showed the half-wave and onset potential for ORR of the catalyst that synthesized at 750 °C surpassed 90 mV over that of 20 wt% Pt/C catalyst. The mechanism for the high catalytic performance was clarified on the basis of the electron transfer from encapsulated Fe_3C to outer layer N-CNT. The additional electron modulated the polarization of C-N bonds in the electric field of Fe_3C and N-CNT. The results of the paper established a novel theory to explain the high catalytic performance for ORR and proposed a novel method to modulate the electron state of carbon based catalysts.

2. Material and methods

2.1. Reagents and materials

Melamine ($C_3H_6N_6$), potassium hydroxide (KOH), Iron(III) chloride ($FeCl_3$) and concentrated sulfuric acid (H_2SO_4) were purchased from Sinopharm Chem. Reagent Co. Ltd (Shanghai, China). Commercial 20 wt% Pt/C catalyst was got from Aladdin Co. Ltd (Shanghai, China). All reagents were in analytically pure states and adopted without any further treatment. All aqueous solutions were prepared by deionized water that was purified by a Milli-Q Lab apparatus (Nihon Millipore, Ltd. China)

2.2. Materials synthesis

The preparation procedure of N-CNT encapsulated Fe_3C are displayed in Fig. S1 (Supporting Information). The obtained catalysts were named as CAT-XX-TTT, where XX meant the different moles of iron chloride and TTT meant the corresponding calcination temperature in centigrade degree. For example, CAT-20-750 meant the catalyst was prepared by using 20 mmol $FeCl_3{\cdot}6H_2O$ and the final calcination temperature was 750 °C. The details for the synthesis and naming rules of the catalysts are provided in Supporting Information.

2.3. Materials characterization

The field emission scanning electron microscopy (SEM) tests were conducted by a Hitachi High-Technologies S-4800 microscope. Transmission electron microscopy (TEM), high resolution TEM (HR-TEM) and high angle angular dark field-scanning transmission electron microscopy (HAADF-STEM) images were taken on JEM-2100F with 200 kV acceleration voltage. X-ray photoelectron spectra (XPS) test results of the catalysts were recorded by a Thermo Fisher K-Alpha equipped with a monochromatic Al Kα X-ray radiation source. The C 1s peak with a precision of 0.02 eV was used as the reference at 284.6 eV. X-ray diffractograms of the catalyst were obtained by using a Focus D8 Powder X-ray diffractometer (Bruke Co. Ltd, Germany) with Cu Kα radiation and graphite monochromator that operated at 40 kV. The scanned 2θ was ranged from 20° to 80° with a step of 0.02°. To measure the specific surface area (S_{BET}) of the catalysts, a Micromeritics ASAP 2020 physical adsorption analyzer was adopted according to the Brunauer–Emmett–-Teller (BET) method using N_2 adsorption at 77.3 K. For BET test, each catalyst was firstly degassed at 350 °C under vacuum for 6 h. Raman spectra of the catalysts were collected at room temperature by a Renishaw in Via Raman microscope with laser excitation of

532 nm. X-ray absorption fine spectroscopy (XAFS) tests at the Fe K-edge were conducted in either transmission or fluorescence modes at the10-BM and 10-ID beam lines with an energy resolution of 150 meV at Institute of High Energy Physics, Chinese Academy of Sciences.

2.4. Electrochemistry tests

Electrochemical measurements were conducted by using a standard three-electrode cell system that was connected with CHI 760D electrochemical workstation (Chenhua Inc., Shanghai, China). A RRDE-3A (RRDE Inc. Japan) system that was coupled with the electrochemical workstation was employed for the rotating disk electrode (RDE) measurements. The electrochemical tests were operated at ambient temperature. The three-electrode system included a glassy carbon RDE (diameter 3 mm) that was covered with the as-prepared catalyst, a graphite electrode and a saturated Hg/Hg_2Cl_2 electrode, which played the role of working electrode, counter electrode and reference electrode. 5.0 mg commercial 20 wt% Pt/C or the catalyst was usually dispersed in a mixed solution of 450 μL DI H_2O and 50 μL Nafion solution (Aldrich, 5 % in aliphatic alcohols) followed with sonication for 1 h to obtain a black ink. Then, 5 μL of the black ink was pipetted onto the surface of the polished glassy carbon electrode and naturally dried to form a membrane.

Cyclic voltammetry (CV) measurements were performed in an oxygen-saturated 0.1 M KOH electrolyte with the potential range from −0.8 to 0.2 V (vs. Hg/Hg_2Cl_2) with the sweeping rate of 50 mV s^{-1}. Linear sweep voltammetry (LSV) tests were recorded at a sweeping rate of 10 mV s^{-1} at the rotating speed of 1600 rpm. The long-time running stability performance for ORR was examined by LSV tests that conducted at initial and after 30 h running at 0.93 V (half-wave potential). RDE tests were conducted with different rotating speeds (from 625 to 2025 rpm) at the sweeping rate of 10 mV s^{-1}. The electrolyte solution was firstly bubbled with O_2 or Ar for 30 min prior to each test to assure the saturation. The ORR current was deduced by subtracting the current of Ar-saturated electrolyte from that of O_2-saturated electrolyte. For the methanol crossover effect test, the chronoamperometric test at 0.6 V (vs RHE) was operated by using RDE tests in oxygen-saturated 0.1 M KOH at the rotating speed of 1600 rpm, following with methanol injection to the concentration of 3 M.

3. Results and discussion

3.1. Structure characterization

The structure of the catalysts that synthesized at 750 °C with different iron content was firstly examined by XRD tests and the obtained results are displayed in Fig. 1A.

On the basis of XRD test results in Fig. 1A, it can be indexed the co-existence of Fe_3C and carbon. The Fe_3C and carbon should be derived from the reaction of melamine and iron chloride during the course of high temperature calcination. The pyrolysis of the mixture of imidazole and iron precursor also formed CNT encapsulating Fe_3C particles structure [18]. In the Ni/Fe catalyzed synthesis of CNT, similar XRD test results were also obtained [19]. Fig. S2 (Supporting Information) showed the XRD patterns of the catalyst that synthesized at 650 °C. The XRD patterns of the catalysts that obtained at 750, 850 and 950 °C with the same iron precursor content are exhibited in Fig. S3 (Supporting Information). The existence of Fe_3C and carbon is also confirmed. Similar results were also observed in

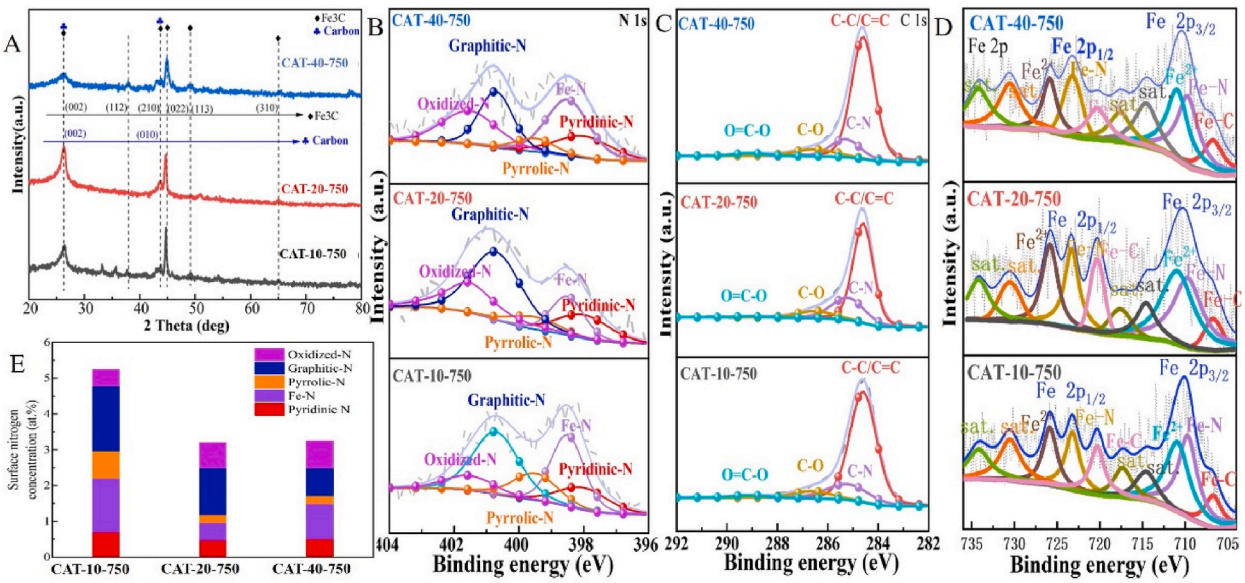

Fig. 1. XRD test results (A), deconvoluted high resolution XPS of nitrogen (B) carbon (C) and iron (D) of CAT-10-750, CAT-20-750 and CAT-40-750 catalysts. (E) Nitrogen species and corresponding content of the catalysts that calculated based on the XPS test results.

the research on nitrogen-coordinated iron-co-doped carbon catalysts for ORR [20,21].

To furtherly investigate the elemental composition of the catalysts, the XPS examinations were conducted and the full spectra XPS of the catalysts that synthesized at 750 °C with different iron precursor content are provided in Fig. S4 (Supporting Information), which distinctly confirmed the coexistence of Fe, N, C and O element. Fig. 1B clearly revealed that the nitrogen combining state of the catalysts was different from each other. The combining energy of the same bond had a slight increase with increasing iron content, which should be resulted from the different combining states of the atoms in the catalysts. The co-existence of the Fe-N bond in the XPS of Fe 2p and N1s confirmed the successful doping of nitrogen to Fe_3C. Similar results were also detected in other researches [22].

Fig. 1C showed the XPS of carbon of the catalysts, which clearly confirmed the existence of C-C/C=C bond that could be attributed to the N-CNT. The C-N bond was also deconvoluted in the XPS of the three catalysts, which should be derived from the precursor of melamine. Research on dual-sided Fe/Fe_3C@N-doped CNTs found that the C 1s spectra were deconvoluted into two types bonds that centered at 284.7 eV and 285.5 eV, which were corresponding to C-C and C-N bond, respectively [23]. The bond of Fe-C should be attributed to Fe_3C that had been proved by the XRD tests. The existence states of carbon in the catalysts were also examined by Raman tests, which were supplied in Fig. S5 (Supporting Information). It is distinctly observed that the I_D/I_G of CAT-20-650 was the highest, which meant that the structure had the highest defects intensity in all the catalysts. The deconvoluted XPS of Fe in Fig. 1D clearly showed that the iron had combined with carbon and nitrogen. The result was consistent with the XPS of nitrogen and carbon. This was why the iron was ever ascertained as the catalysts for the formation of N-CNT [24]. In this paper, the N-doped Fe_3C first played the catalytic role for the synthesis of N-CNT. Researches on the hetero-structural interfaced Fe_3C-TiN catalysts also detected the Fe-C bond

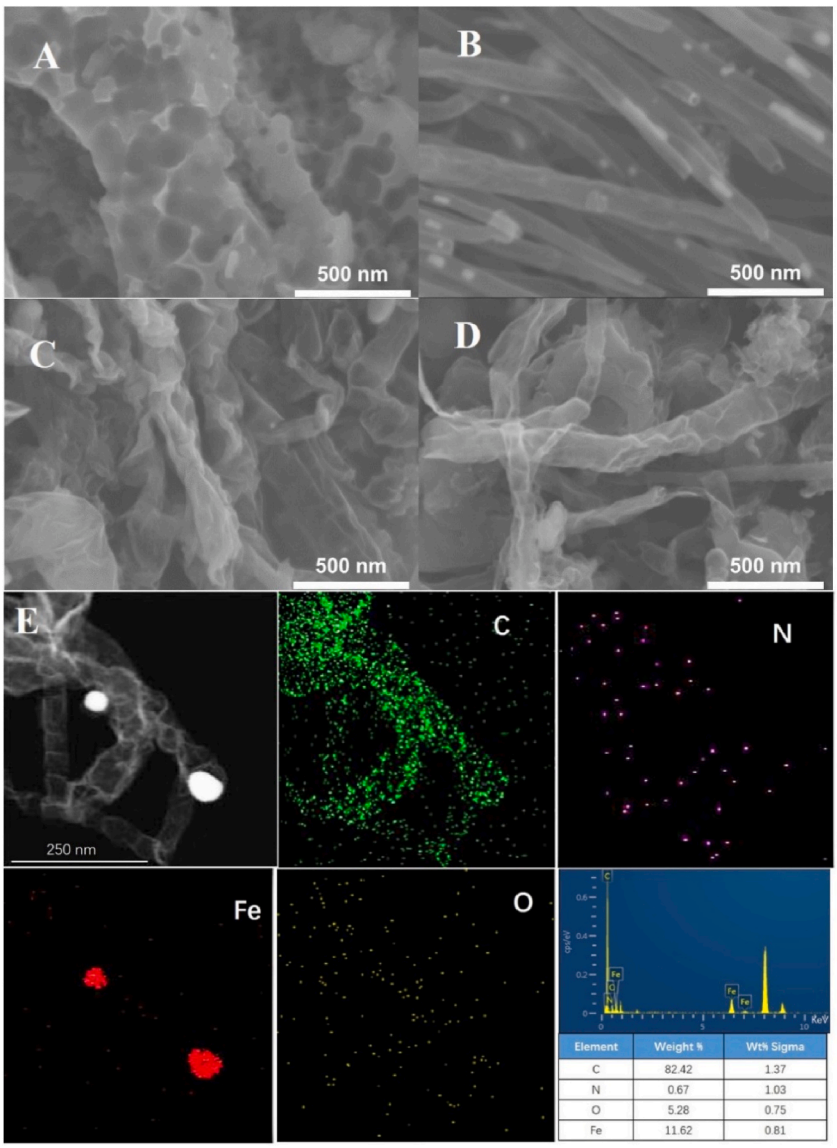

Fig. 2. SEM tests of (A) CAT-20-650, (B) CAT-20-750, (C) CAT-20-850 and (D) CAT-20-950. (E) TEM and elemental mapping tests of CAT-20-750.

[25]. Similar XPS peaks fitting results had also been reported by M.R. Linford [26].

Fig. 1E showed the nitrogen species and corresponding content in the catalysts. It could be seen that the nitrogen combined with iron and carbon. Combining with the XRD patterns, it can be known that the nitrogen-iron bond should be originated from the doped nitrogen of Fe_3C. The C-N bonds were deconvoluted into graphitic-nitrogen, pyrrolic-nitrogen, pyridinic-nitrogen and oxygen-nitrogen, which played different roles on the catalytic performance for ORR [27]. To furtherly evaluate the catalyst structure, the SEM tests were performed and the obtained results are displayed in Fig. 2.

Comparison between Fig. 2A to D showed that the morphology of the materials was greatly influenced by the calcination temperatures. Fig. 2A showed the material that calcined at 650 °C displayed a multi-hole stick state. This should be resulted from the heat-treating temperature that made the melamine pyrolyzed intermediate disintegrate again and eventually formed the morphology. Fig. 2B clearly showed a perfect nanotube structure with some particles encapsulated in the tube or plugged on the top when the material was calcined at 750 °C. Similar structure were also observed in the research of potassium chloride catalyzed synthesis of porous carbon nanotube [28]. Fig. 2C and D displayed that the catalysts with calcination temperature of 850 and 950 °C also formed nanotube structure. Comparison of Fig. 2B, C and 2D revealed that the surface of the catalysts gradually become coarse with elevating calcination temperature.

Fig. 2E showed the TEM tests and elemental mapping of CAT-20-750, which clearly showed that the Fe_3C particles located on the top of the few walled nanotubes. Researches on the bottom-up synthesis of carbon nanotubes also found the similar structure of iron catalysts adherent on the bottom of CNT [29]. The results were also consistent with that of Ketjenblack that incorporated into Fe/Fe_3C-functionalized melamine foam [30]. Fig. 2E also clearly confirmed nanotube structure of the catalysts. The corresponding elemental mapping of C, N, Fe and O also proved the doping of nitrogen to carbon nanotube and Fe_3C. On the other hand, the corresponding elemental ratio of the catalysts was also provided. The formation of N-CNT and Fe_3C were also proved by the XPS and elemental mapping test results. As comparison, the TEM test results and corresponding elemental mapping of the CAT-40-750 are provided in Fig. S6 (Supporting Information). The existence of nitrogen was also proved by FT-IR tests that provide in Fig. S7 (Supporting Information), which also displayed a N-CNT encapsulating Fe_3C structure. Similar conclusion was also derived in the research of one-pot synthesis of CNT [31]. Combining with the XSP and SEM test results, the nitrogen contents of the catalysts are drawn and provided in Table S1.

The SEM of the catalysts in Fig. 3A, D and 3G exhibited a nanotube structure. Some particles were also observed. The HAADF-STEM test result in Fig. 3B, E and 3H displayed that the nanotube had a few wall structure. The diagrams also revealed that the Fe_3C particles were encapsulated in the N-CNT or located on the top of N-CNT. The iron based metastable compound catalyzed the formation of N-CNT. Similar phenomena were also observed in the research of Co-CNT systems [32]. Transitional metals that can form metastable compounds react with carbon resource firstly and then forming CNT on the active sites, which can promote the deposition of carbon and form carbon with kinds of morphology. The synthesis of thin wall carbon nanotubes filled with micrometer-length Fe_3C particles or empty thin wall CNT tip-filled with Fe_3C were controlled by the precursor [33]. The shape of the CNT was also influenced by nitrogen atoms that derived from melamine [34]. The increased nitrogen content affect both the nucleation and growth of CNT.

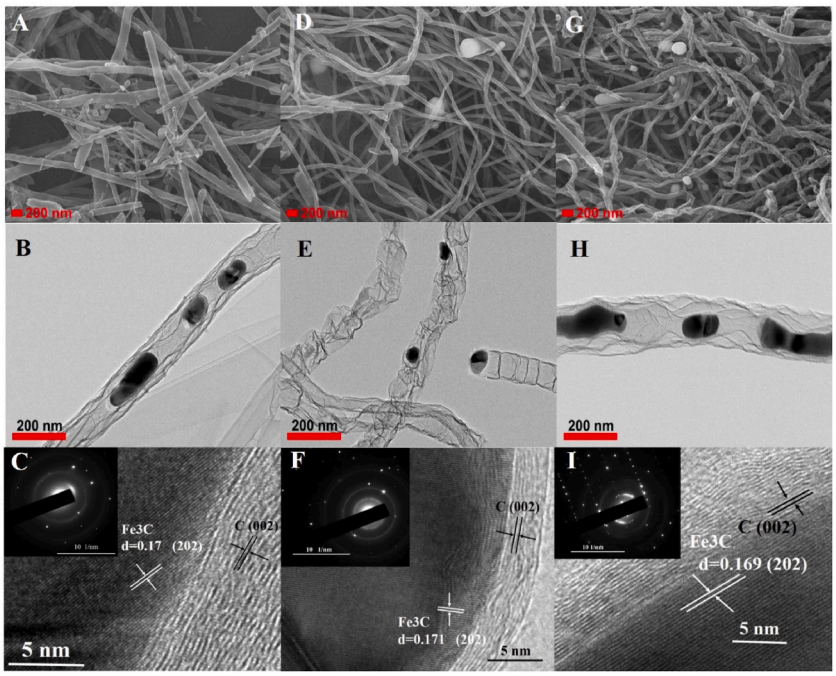

Fig. 3. (A)(B)(C), (D)(E)(F) and (G)(H)(I) are the SEM and two HAADF-STEM test results of CAT-10-750, CAT-20-750 and CAT-40-750, respectively. The inset in (C), (F) and (I) are the corresponding SAED test results.

The doped nitrogen reduced the catalyst/CNT surface energy, reduced carbon extrusion from the catalyst and CNT growth rate, reduced catalyst motion and stabilized catalyst morphology in the process of growth. The iron also played the effect of catalysts during the synthesis of single wall CNT [35]. The transformation between the state of Fe, C and Fe_3C greatly influenced the growth of N-CNT. The structure of the Fe_3C@N-CNT that synthesized at different temperatures was also examined by BET tests and the results are provided in Figs. S8 and S9 (Supporting Information), respectively. The obtained specific surface area, micro-volume and pore volume of the catalysts are provided in Table S2 (Supporting Information). Table S2 distinctly showed that the CAT-20-750 exhibited the

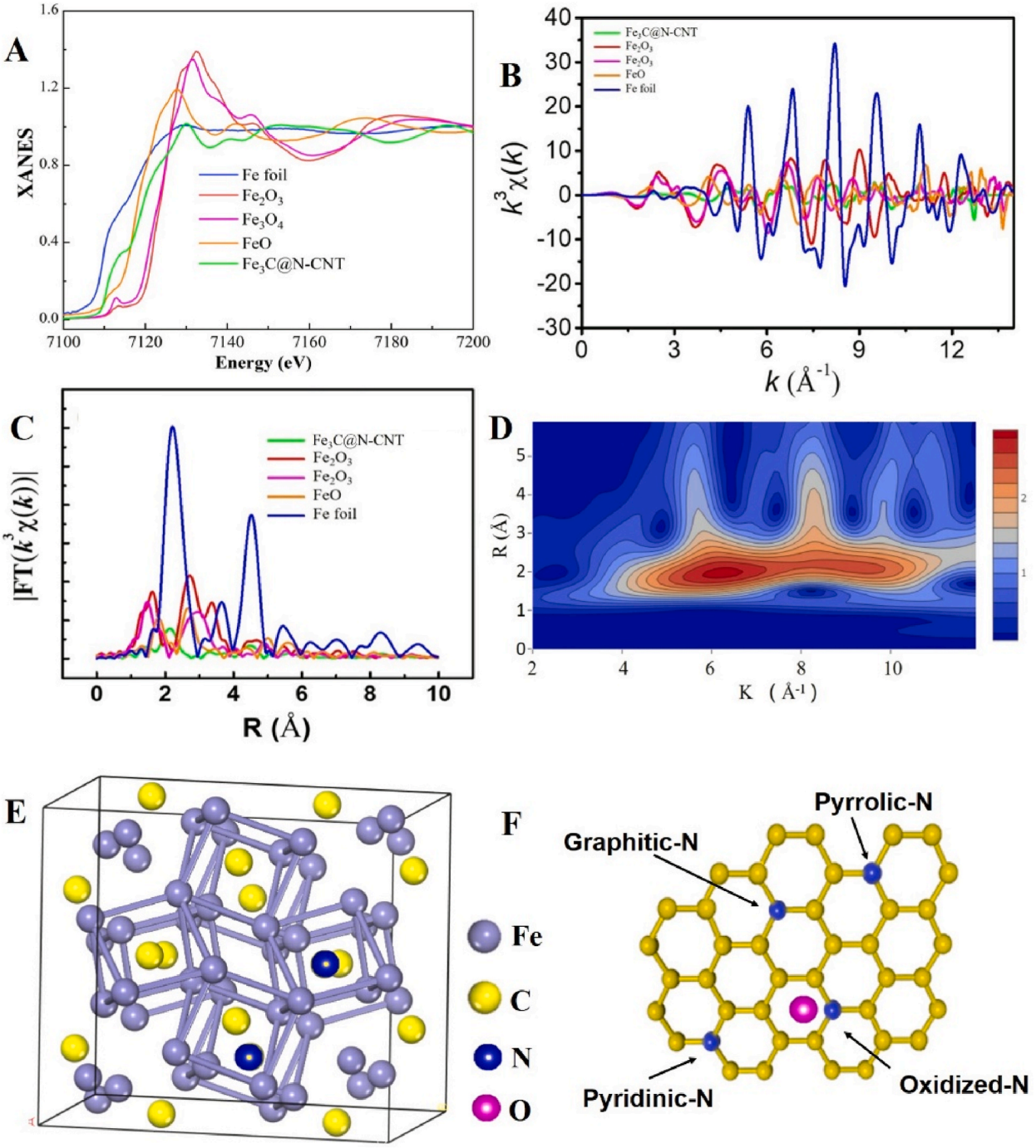

Fig. 4. (A) Fe *K*-edge X-ray absorption near-edge structure (XANES) spectra. (B) The corresponding k^3x (*k*) and (C) the corresponding Fe *K*-edge Fourier transform (FT) k^3-weighted x (*k*)-function of Fe_3C@N-CNT, Fe_2O_3 Fe_3O_4, FeO and Fe foil. (D) Wavelet transforms (WT) of Fe_3C@N-CNT. (E) The atomic structure of Fe_3C. (F) The modulated structure of N-occupied positions of surface layer CNT.

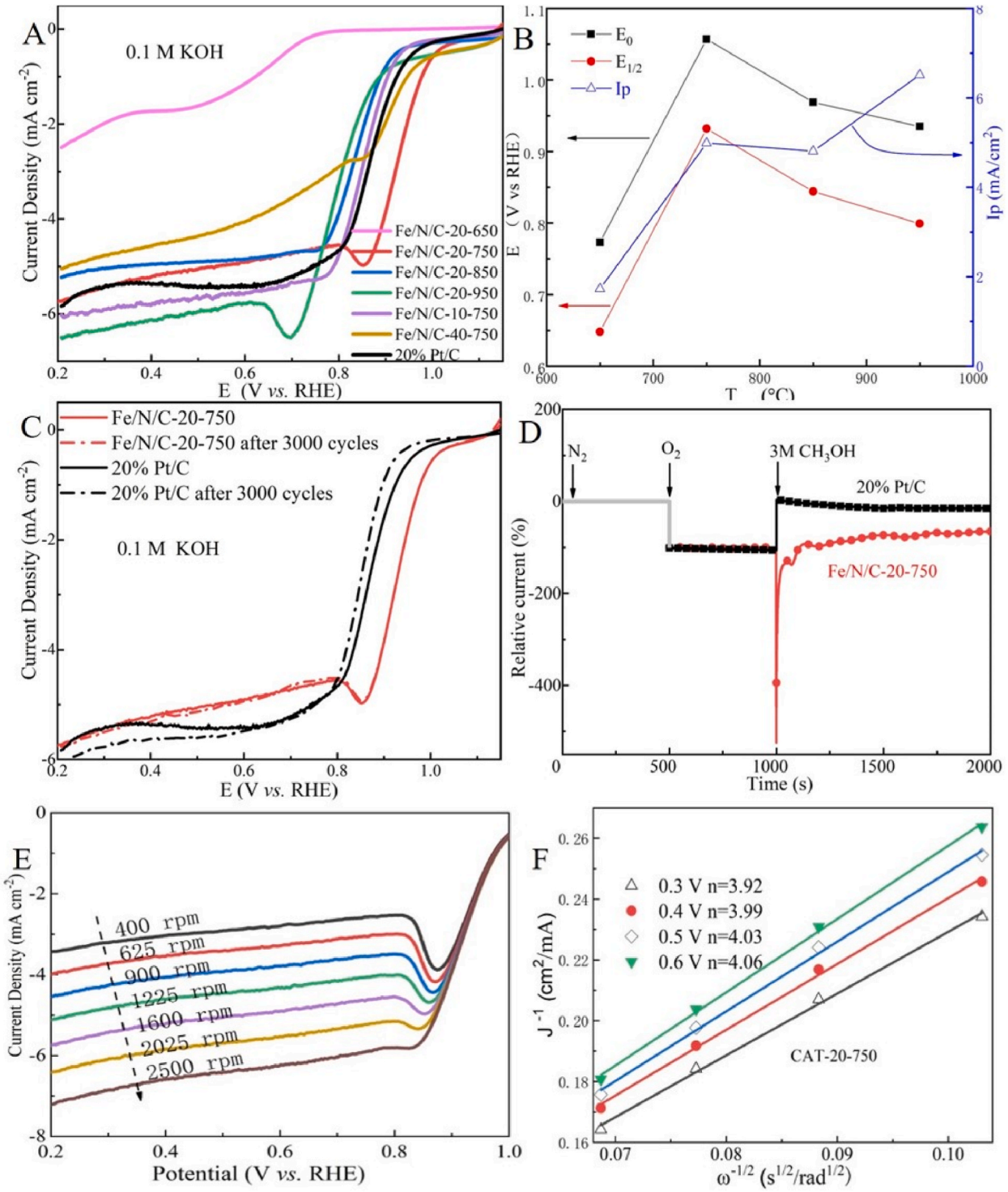

Fig. 5. (A) LSV test results of the catalysts with different synthesis iron content and different calcination temperature. (B) The dependence of peak current intensities (*Ip*), onset potential (E_0) and half-wave potential ($E_{1/2}$) to calcination temperature of the catalysts with same iron precursor content in 0.1 M KOH. (C) The LSV tests of CAT-20-750 and Pt/C catalysts at initial and after 30 h continuous running at 0.93 V. (D) The current-time tests with the poisoning of methanol of CAT-20-750 and Pt/C catalysts. (E), (F) are the RDE and corresponding K-L line of CAT-20-750 catalyzed ORR in 0.1 M KOH electrolyte.

highest specific surface area. Fig. 3C, F and 3I showed the HAADF-STEM tests of the N-CNT encapsulated Fe_3C catalyst. The lattice distance of 0.17 nm was captured by the HAADF-STEM tests, which was corresponding to the (202) facet of Fe_3C. Similar structures were also detected in the research of Co_3Fe_7-Fe_3C based catalysts for ORR [36]. The insets in Fig. 3C, F and 3I were the corresponding SAED test results that also confirmed the existence of Fe_3C. To furtherly investigate the coordination structure of Fe at the atomic level of the catalysts, the X-ray cabsorption fine structure (XAFS) measurements were operated and the obtained results are showed in Fig. 4.

Fig. 4A exhibited the Fe *K*-edge X-ray absorption near-edge structure (XANES) spectra of Fe_3C@N-CNT, Fe_2O_3 Fe_3O_4, FeO and Fe foil. The spectra of CAT-20-750 is very similar to that of reference Fe foil. The near-edge absorption energy of Fe_3C@N-CNT located between the values of Fe and FeO and shifted to higher energy area than Fe foil, which should be caused by the different electronegativity of carbon and oxygen atoms. The electronegativity of carbon was lower than that of oxygen. Researches on single atomic Fe based catalysts drew similar conclusion [37]. Fig. 4B showed the k^3x (k) curves of Fe_3C@N-CNT, Fe_2O_3, Fe_3O_4, FeO and Fe foil in k space. Similar results were also obtained in the research on the coordination environment of the Fe_2 site for the Fe_2/g-C_3N_4 precursor and the Fe_2-DAC catalyst as $N_4[Fe_2(m\text{-}O(H))_2]$ and $N_4[Fe_2(m\text{-}N)_2]$ configuration, respectively [38]. The intensity of Fe_3C@N-CNT located between Fe and FeO, which proved the combination of Fe and C.

Fig. 4C showed the Fourier Transform (FT) k^3-weighted extended X-ray absorption fine structure (EXAFS) spectra of Fe_3C@N-CNT, Fe_2O_3, Fe_3O_4, FeO and Fe foil. The EXAFS tests of Fe_3C based catalysts for ORR suggested that Fe in the samples was major in a local coordination environment, which was quite similar to that of Fe(III)pc (i.e., FeN_4Ox) [39]. Researches on the Fe K-edge X-ray absorption of Fe foil, Fe_3C, etc. also revealed that the structure of Fe_3C was quite similar to Fe [40]. Combining with the TEM and elemental mapping tests, it could be deduced that the nitrogen was also doped into the crystallinity of Fe_3C. Researches on the catalytic sites of iron- and nitrogen-doped graphene materials ascertained the distance of Fe-N by XANES tests [41].

To distinguish the Fe-C and Fe-N bonds, the wavelet transform (WT) tests were carried out to examine the Fe K-edge EXAFS oscillations of Fe_3C@N-CNT, Fe_2O_3, Fe_3O_4, FeO and Fe foil. Fig. 4D showed that the WT of Fe_3C@N-CNT major located between the k value of 4.2 $Å^{-1}$ and 10.6 $Å^{-1}$. To compared with the WT of Fe_3C@N-CNT, the WT of Fe_3O_4, Fe_2O_3, FeO and Fe foil were listed in Fig. S10 (Supporting Information). It could be found that the WT value of Fe_3C@N-CNT was stronger than that of Fe foil, which located between 5.8 $Å^{-1}$ and 10.5 $Å^{-1}$. Combined with XPS test results, the changes of WT could be assigned to Fe-C bonds. In the research of cobalt based catalysts, the WT changes were attributed to the Co-N_4 coordinated sites [11]. This also proved the successful doping of nitrogen to Fe_3C particles that was consistent with the XPS test result.

On the basis of the XANES test result, the structure of N-doped Fe_3C of Fe_3C@N-CNT was modulated and displayed in Fig. 4E. The nitrogen and carbon atoms connected with iron atoms. On the other hand, the nitrogen and carbon also made interactions with each other. Nitrogen and carbon atoms with higher negativity attracted electron from iron atoms and formed a negative-charged state. Thus, the iron atoms were in positive state. The electrons were furtherly tranfered along the outer layer N-CNT and eventually formed an electric field along the axis of the Fe_3C and N-CNT. The additional electrons that shifted from Fe_3C of the N-CNT furtherly influenced the C-N boond, which eventually modulated the catalytic acticity for ORR.

Fig. 4F showed the structure of surface layer N-CNT with different doped nitrogen atoms. Combined with the XPS and XANES tests, it could be deduced that the doped nitrogen occupied the graphitic, pyrrolic, pyridinic and oxygenated positions. Nitrogen with different position had different electronic state, which eventually influenced the ORR on the surface.

3.2. *Electrocatalytic characterization for ORR of Fe_3C@N-CNT*

The electrocatalytic performance of the catalysts for ORR were firstly examined in 0.1 M KOH electrolyte by cyclic voltammetry (CV) tests and the obtained results are provided in Fig. S11 (Supporting Information). Then, the performance of the fully activated catalysts were examined by linear scanning votammetry (LSV) tests and the obtained results are supplied in Fig. 5A.

Fig. 5A showed the LSV test results of all the synthesized catalysts. It was clearly revealed that the CAT-20-750 displayed the highest onset potential for ORR, which even 90 mV higher than that of the 20 wt% Pt/C catalyst. It is also observed that the peak current intensity of CAT-10-750 and CAT-20-950 surpassed that of the 20 wt% Pt/C catalyst. Researches on the Fe/N co-doped hierarchically porous N-doped CNT towards ORR obtained similar results [42]. Fig. 5A also clearly showed that the CAT-20-650 displayed the lowest catalytic performance in all the catalysts. This could be induced from the structure that had not fully crystallized into CNT. Based on the LSV tests of Fig. 5A, the onset potential (E_0) and half-wave potential ($E_{1/2}$) of the catalysts that prepared with 20 mmol Fe precursor and calcined at 750, 850 and 950 °C for ORR were obtained and displayed in Fig. 5B. It is obviously exhibited that the E_0 and $E_{1/2}$ of the catalysts were slightly decreased with the elevating calcination temperature. The changes of the potential and current should be attributed to the nitrogen content of the surface layer CNT that made great influences on the active center and electron distribution.

Fig. 5C distinctly revealed that the E_0 and $E_{1/2}$ of CAT-20-750 was about 90 mV higher than that of 20 wt% Pt/C catalyst. This revealed the high catalytic activity of CAT-20-750 catalyst. Compared with the reported catalytic performance pristine N-CNT [43], it can be deduced that the encapsulated Fe_3C played crucial role on enhancing the catalytic performance towards ORR of CNT. The encapsulated Fe_3C provided additional electrons to surface layer N-CNT. On the other hand, with the introduction of additional electrons, the polarization of C-N bond in the surface layer N-CNT was changed. The encapsulated Fe_3C and surface layer N-CNT formed an additional electric field along the axis that made great influences on the intermediate molecular movement and eventually improved the $E_{1/2}$ and E_0 of Fe_3C@N-CNT catalyzed ORR.

It could also be seen from Fig. 5C that the LSV test results of the Pt/C and CAT-20-750 at initial and after 30 h continuous running at 0.93 V. It is distinctly proved that there were even no changes observed on the catalytic performance of CAT-20-750, which should be attributed to the encapsulation of the N-CNT that prevent the corrosion of the Fe_3C. It is also revealed that the half-wave potential of

20 wt% Pt/C catalyzed ORR decreased about 30 mV after continuous running 30 h. Similar phenomena were ever observed in the research on Co@N-CNT catalysts for ORR [44]. Researches on N-CNT array based catalysts for ORR attributed the high catalytic performance to the incorporation of electron-accepting nitrogen atoms in the conjugated CNT plane [45]. The nitrogen atoms attracted electrons from adjacent carbon atoms that made the carbon in a relatively positive charge state. Researches on Fe@C_2N catalyzed ORR attributed the catalytic performance to electron tunneling of the inner Fe-based core to the surface of the graphite nitride shell of Fe@C_2N nanoparticles [46]. The enhanced ORR catalytic performance had also been assigned to surface quinones (and/or other possible oxygen functionalities) in the outer layer CNT [47]. Researches on the S and N coordinated Fe atomic sites (FeN_3S) catalysts confirmed that the interaction between Fe, N and S induced electron redistribution, which lowered the binding strength of oxygenated reaction intermediates and eventually enhanced the reaction kinetics and catalytic performance towards ORR [48]. Electrocatalytic properties of the N-doped wood-derived carbon based catalysts were attributed to the enlarged surface area, specific ratio of micro- and meso-pores, as well as the high percentage of pyridinic nitrogen [49]. Density functional theory calculations revealed that the adsorption of ORR intermediates on the basal carbon of the pristine CNTs significantly enhanced the adsorption energy, which could be detected on the similar positions of two types of typical intramolecular junction structures (straight and bent junctions) with the values close to Pt (111) facet [50]. Atomic Fe and N co-doped mesoporous carbon nano-spheres also exhibited excellent catalytic activity and durability towards ORR, which was attributed to the highly opened structure and hydrophobic surface [51]. It had ever been reported that the electron transferring from encapsulated Fe_3C to outer layer N-CNT played important role on enhancing the electrocatalytic performance for ORR of CAT-20-750. The CV tests in non-faradic and corresponding ECSA calculation, and electrochemical impedance spectroscopy (EIS) test results of CAT-20-650, CAT-20-750, CAT-20-850, CAT-20-950 that are displayed in Figure S12, S13 and S14 (Supporting Information), also proved the robust catalytic performance of CAT-20-750.

Fig. 5D displayed the anti-poison performance of Pt/C and CAT-20-750 catalysts. It is clearly observed that, at the initial 1000 s, the performance of the Pt/C and CAT-20-750 catalyst keep constant. With the introduction of methanol to electrolyte, the current intensity of the Pt/C catalyst great decreases. This should be resulted from the methanol poison of the Pt/C catalyst. As contrast, the current of CAT-20-750 catalyzed ORR was firstly increased and then recovered to the normal level. It seemed that the addition of methanol made no influences on the catalytic performances of the CAT-20-750 catalyst. The 3D ordered macro-porous graphitic C_3N_4/carbon composite also exhibited higher anti-poison performances than Pt/C catalyst [52]. The long-time running stability of catalyst should be attributed to two factors. The first factor is the shelter of the N-CNT to the Fe_3C. The shelter of outer layer N-CNT prevent the direct contact between Fe_3C and methanol, which can keep the number of active catalytic site constant. The second factor is that the N-CNT with lower affinity to methanol. The polarization of the C-N bond cannot produce high enough absorption to methanol. The two factors assured the high long-time running stability of the CAT-20-750 catalyst. Similar results have ever been observed in the research of super-capacitors [53]. To furtherly investigate the catalytic performance of CAT-20-750 for ORR, the rotate disc electrode (RDE) tests were conducted and the obtained results are displayed in Fig. 5E.

Fig. 5E exhibited the RDE test results of CAT-20-750 catalyzed ORR in 0.1 M KOH electrolyte. It is clearly observed that the current intensity improved with the increase of rotating speeds, which should be attributed to the promoted oxygen diffusion on the electrode surface [54]. Fig. 5F exhibited the corresponding *K-L* lines for the calculation of electron transfer numbers (*n*) according to equations (2) and (3) in Supporting Information. The calculated value of *n* was about 4 that meant the ORR major happened in the style of 4-electron pathway [55], which also confirmed the high catalytic activity for ORR of CAT-20-750. The RDE tests and corresponding *K-L* lines of Pt/C catalyzed ORR in 0.1 M KOH are provided in Figs. S15 and S16 (Supporting Information), which also prove that the ORR major happened by 4-electron pathway. The Tafel test results of Pt/C and CAT-20-750 in Fig. S17 (Supporting Information) prove that the polarization of CAT-20-750 catalyzed ORR is weaker than that of the Pt/C catalyst. Investigation on LSV, RDE, EIS and Tafel tests proved that the catalytic activity of CAT-20-750 surpassed that of the Pt/C catalyst. The mechanism for the high catalytic performance towards ORR of Fe_3C@N-CNT is illustrated in Fig. 6.

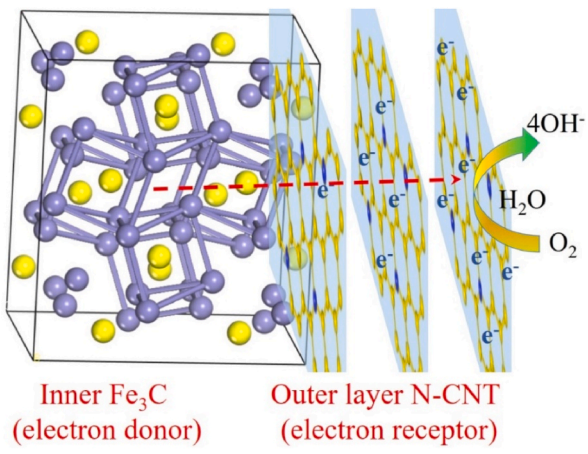

Fig. 6. The mechanism of Fe_3C@N-CNT catalyzed ORR. The Fe_3C particles was encapsulated by N-doped few-layered CNT through eutectic carbon atoms. Modulated structure of encapsulating and the ORR process on the surface.

The in-situ derived N-CNT acted as active sites for ORR, which contributed to the most of the ORR process [56]. Researches on the catalytic performance of Co-embedded CNT attributed the high ORR catalytic activity to higher pyridinic-N content [57]. The XPS test results in Fig. 1E showed that the pyridinic-N content of CAT-20-750 was 0.5 wt%, which provided enough catalytic active center for ORR. Researches on electrocatalytic deuteration attributed the improvement of faradaic efficiency to nanotip-enhanced electric field of metal catalysts [58]. The carbon radical intermediates played important role on the improvement of deuteration efficiency. In this paper, the carbon and doped nitrogen shows higher electron transfer efficiency for ORR under the electric fields of encapsulated Fe_3C. On the other hand, the inner layer carbon nanotube of the encapsulation structure provided facilitate channels for electron transfer that eventually improved the catalytic activity of CAT-20-750 for ORR in alkaline electrolyte. The inner layer N-CNT provide a fast electron transfer channel between the encapsulated Fe_3C and outer layer N-CNT. Then the additional electrons formed an electric field along the axis of N-CNT [59]. It is usually believed that the ORR major happened on the catalysis of doped nitrogen. The effect of iron compound or composite are also the catalytic active site for ORR. But the result show that the encapsulated Fe_3C can also play vital role on improving the catalytic performance, which avoid the direct contact between active metal composites and the reactant, such as oxygen, electrolyte and other materials. The encapsulation can keep the high activity and ong-time working stability of catalyst. The electric field determined the electron state of C-N bonds of outer layer N-CNT, which eventually enhanced the catalytic activity for ORR.

4. Conclusion

In this paper, one kinds of few layered N-CNT with Fe_3C encapsulated catalyst were successfully synthesized, which were proved by HAADF-STEM and XANES tests. The encapsulated Fe_3C and outer layer N-CNT tightly connected through transition layers. The high catalytic performances for ORR were investigated by LSV, CV, EIS, Tafel and RDE tests. The onset potential and half-wave potential of CAT-20-750 catalyzed ORR surpassed 90 mV over that of 20 wt% Pt/C catalyst. Combined with the other researches on CNT encapsulated metal or metal oxide based catalysts, it can be deduced that the catalytic performance of CNT can be modulated through additional electron supplication. The encapsulated Fe_3C and the N-CNT formed electric field along the axis of the capsulation structure, which promote the shift of electron from Fe_3C to outer layer N-CNT. The additional electronics furtherly modulated the state of N-C bonds that eventually elevated the onset potential, half-wave potential and maximum current of catalyzed ORR in alkaline electrolyte. The results of the paper provide a novel methodology to design high performance and low-cost CNT based ORR catalysts through forming additional electron providing centers.

CRediT authorship contribution statement

Jun Dong: Writing – review & editing, Project administration. **Qiqi Jiao:** Resources, Methodology, Formal analysis. **Hao Wang:** Resources, Funding acquisition, Data curation. **Hong Wang:** Validation, Software, Investigation. **Yi-ke Ren:** Software, Resources, Data curation.

Declaration of competing interest

The authors declare that they have no known competing financial interests or personal relationships that could have appeared to influence the work reported in this paper.

Acknowledgements

This work is financially supported by National Natural Science Foundation of China (No. 22075290), Clinical Medical Science and Technology Innovation Plan of Jinan (202019165).

Appendix A. Supplementary data

Supplementary data to this article can be found online at https://doi.org/10.1016/j.heliyon.2024.e40862.

The encapsulated Fe3C provides electron to outer layer N-CNT and forms electric field along the axis that enhances the happening of ORR on C-N.

References

[1] H. Li, S. Kelly, D. Guevarra, Z. Wang, Y. Wang, J.A. Haber, M. Anand, G.T.K.K. Gunasooriya, C.S. Abraham, S. Vijay, J.M. Gregoire, J.K. Nørskov, Analysis of the limitations in the oxygen reduction activity of transition metal oxide surfaces, Nat. Catal. 4 (2021) 463–468.

[2] M.Y.a.M. Yan, Monitoring and early warning analysis of the epidemic situation of Escherichia coli based on big data Technology and cloud computing, J Healthc Eng 2022 (2022) 8739447.

[3] R. Nandan, P. Pandey, A. Gautam, O.Y. Bisen, K. Chattopadhyay, M.M. Titirici, K.K. Nanda, Atomic arrangement modulation in CoFe nanoparticles encapsulated in N-doped carbon nanostructures for efficient oxygen reduction reaction, ACS Appl. Mater. Interfaces 13 (2021) 3771–3781.

[4] Z. Zhou, Z. Zhang, L. Su, M. Yang, M. Hu, J. Bao, J. Wei, A composite of Co nanoparticles highly dispersed on N-rich carbon substrates: an efficient electrocatalyst for Li-O2 battery cathodes, Chem. Commun. 50 (2014) 776–778.
[5] Y. Liang, H. Wang, J. Zhou, Y. Li, J. Wang, T. Regier, H. Dai, Covalent hybrid of spinel manganese–cobalt oxide and graphene as advanced oxygen reduction electrocatalysts, J. Am. Chem. Soc. 134 (2012) 3517–3523.
[6] N. Li, R.G. Hadt, D. Hayes, L.X. Chen, D.G. Nocera, Detection of high-valent iron species in alloyed oxidic cobaltates for catalysing the oxygen evolution reaction, Nat. Commun. 12 (2021) 4218.
[7] T. Huang, S. Mao, H. Pu, Z. Wen, X. Huang, S. Ci, J. Chen, Nitrogen-doped graphene-vanadium carbide hybrids as a high-performance oxygen reduction reaction electrocatalyst support in alkaline media, J. Mater. Chem. A 1 (2013) 13404–13410.
[8] T. Huang, S. Mao, G. Zhou, Z. Wen, X. Huang, S. Ci, J. Chen, Hydrothermal synthesis of vanadium nitride and modulation of its catalytic performance for oxygen reduction reaction, Nanoscale 6 (2014) 9608–9613.
[9] S.M. Zhang, M.H. Chen, X. Zhao, J.L. Cai, W. Yan, J.C. Yen, S.L. Chen, Y. Yu, J.J. Zhang, Advanced noncarbon materials as catalyst supports and non-noble electrocatalysts for fuel cells and metal-air batteries, Electrochem. Energy Rev. 4 (2021) 336–381.
[10] L. Jiao, J. Li, L.L. Richard, Q. Sun, T. Stracensky, E. Liu, M.T. Sougrati, Z. Zhao, F. Yang, S. Zhong, H. Xu, S. Mukerjee, Y. Huang, D.A. Cullen, J.H. Park, M. Ferrandon, D.J. Myers, F. Jaouen, Q. Jia, Chemical vapour deposition of Fe–N–C oxygen reduction catalysts with full utilization of dense Fe–N4 sites, Nat. Mater. 20 (2021) 1385–1391.
[11] S. Yang, Y. Yu, M. Dou, Z. Zhang, F. Wang, Edge-functionalized polyphthalocyanine networks with high oxygen reduction reaction activity, J. Am. Chem. Soc. 142 (2020) 17524–17530.
[12] D.M. Morales, M.A. Kazakova, S. Dieckhofer, A.G. Selyutin, G.V. Golubtsov, W. Schuhmann, J. Masa, Trimetallic Mn-Fe-Ni oxide nanoparticles supported on multi-walled carbon nanotubes as high-performance bifunctional ORR/OER electrocatalyst in alkaline media, Adv. Funct. Mater. 30 (2020) 1905992.
[13] T. Huang, H. Fang, S. Mao, J. Yu, L. Qi, In-situ synthesized TiC@CNT as high-performance catalysts for oxygen reduction reaction, Carbon 126 (2018) 566–573.
[14] E.J. Askins, M.R. Zoric, M. Li, Z. Luo, K. Amine, K.D. Glusac, Toward a mechanistic understanding of electrocatalytic nanocarbon, Nat. Commun. 12 (2021) 3288.
[15] U. Martinez, J.H. Dumont, E.F. Holby, K. Artyushkova, G.M. Purdy, A. Singh, N.H. Mack, P. Atanassov, D.A. Cullen, K.L. More, M. Chhowalla, P. Zelenay, A. M. Dattelbaum, A.D. Mohite, G. Gupta, Critical role of intercalated water for electrocatalytically active nitrogen-doped graphitic systems, Sci. Adv. 2 (2016) e1501178.
[16] X.J. Guo, X.Y. Gan, Y. Wang, X.X. Lv, F.X. Wang, S.X. Wang, S. Peng, MOF-derived oxygen vacancy-rich Co/CoO@NC-CNTs hybrid electrocatalyst for oxygen reduction reaction, Chemnanomat 9 (2023) e202200521.
[17] L.N. Lu, Y.L. Luo, H.J. Liu, Y.X. Chen, K. Xiao, Z.Q. Liu, Multivalent CoSx coupled with N-doped CNTs/Ni as an advanced oxygen electrocatalyst for zinc-air batteries, Chem Eng J 427 (2022) 132041.
[18] X. Qiao, J. Jin, J. Luo, H. Fan, L. Cui, W. Wang, D. Liu, S. Liao, In-situ formation of N doped hollow graphene Nanospheres/CNTs architecture with encapsulated Fe_3C@C nanoparticles as efficient bifunctional oxygen electrocatalysts, J Alloy Compd 828 (2020) 154238.
[19] V. Jourdain, M. Paillet, R. Almairac, A. Loiseau, P. Bernier, Relevant synthesis parameters for the sequential catalytic growth of carbon nanotubes, J. Physical Chemistry B 109 (2005) 1380–1386.
[20] H.S. Yoon, H.-Y. Park, W.S. Jung, Synergistic effects of fluorine and nitrogen dopants in fluorine/nitrogen-coordinated iron-co-doped carbon catalysts for enhanced oxygen reduction in alkaline media, Int. J. Hydrogen Energy 60 (2024) 1092–1100.
[21] Y. Zhang, X. Jing, X.-h. Yan, H.-l. Gao, K.-z. Gao, Y. Cao, S. Hu, Y.-y. Zhang, Rational design of NiMn-based electrode materials for high-performance supercapacitors, Coordin Chem Rev 499 (2024) 215494.
[22] Z. Li, X. Liang, Q. Gao, H. Zhang, H. Xiao, P. Xu, T. Zhang, Z. Liu, Fe, N co-doped carbonaceous hollow spheres with self-grown carbon nanotubes as a high performance binary electrocatalyst, Carbon 154 (2019) 466–477.
[23] W.W. Xie, T.Z. Tian, M. Yang, N.W. Li, L. Yu, Formation of hollow frameworks of dual-sided Fe/Fe_3C@N-doped carbon nanotubes as bifunctional oxygen electrocatalyst for Zn-air batteries, Appl. Catal. B Environ. 317 (2022) 121760.
[24] Y. Segawa, A. Yagi, K. Matsui, K. Itami, Design and synthesis of carbon nanotube segments, Angew. Chem. Int. Ed. 55 (2016) 5136–5158.
[25] K.Q. Li, C.Q. Wang, H.X. Li, Y.L. Wen, F. Wang, Q.Y. Xue, Z.Y. Huang, C.P. Fu, Heterostructural interface in Fe3C-TiN quantum dots boosts oxygen reduction reaction for Al-air batteries, Acs Appl Mater Inter 13 (2021) 47440–47448.
[26] J.W. Pinder, G.H. Major, D.R. Baer, J. Terry, J.E. Whitten, J. Čechal, J.D. Crossman, A.J. Lizarbe, S. Jafari, C.D. Easton, J. Baltrusaitis, M.A. van Spronsen, M. R. Linford, Avoiding common errors in X-ray photoelectron spectroscopy data collection and analysis, and properly reporting instrument parameters, Applied Surface Science Advances 19 (2024) 100534.
[27] Y. Sun, R. Zhong, H. Zhang, T. Huang, J. Yu, H. Fang, D. Liang, Z. Guo, Soybean milk derived carbon intercalated with reduced graphene oxide as high efficient electrocatalysts for oxygen reduction reaction, Int. J. Hydrogen Energy 44 (2019) 21790–21802.
[28] S. Lv, L. Ma, X. Shen, H. Tong, Potassium chloride-catalyzed growth of porous carbon nanotubes for high-performance supercapacitors, J Alloy Compd 906 (2022) 164242.
[29] R. Jasti, C.R. Bertozzi, Progress and challenges for the bottom-up synthesis of carbon nanotubes with discrete chirality, Chem. Phys. Lett. 494 (2010) 1–7.
[30] J.-S. Lee, G.S. Park, S.T. Kim, M. Liu, J. Cho, A highly efficient electrocatalyst for the oxygen reduction reaction: N-doped Ketjenblack incorporated into Fe/Fe3C-functionalized melamine foam, Angew. Chem. 125 (2013) 1060–1064.
[31] J. Ma, Y. Ma, F. Yu, A novel one-pot route for large-scale synthesis of novel magnetic CNTs/Fe@C hybrids and their applications for binary dye removal, Acs Sustain Chem Eng 6 (2018) 8178–8191.
[32] F. Bao, C.Y. Hu, Y.K. Huang, H.C. Liu, T. Zhu, G.T. Cong, J.L. Yu, C.Z. Zhu, J. Xu, M.W. Ji, Co nanoparticles/N-doped carbon nanotubes: facile synthesis by taking Co-based complexes as precursors and electrocatalysis on oxygen reduction reaction, Colloid. Surface. 653 (2022) 129912.
[33] J. Guo, Y. He, L. Mu, S. Wang, Z. Weng, G. Xiang, F.S. Boi, The role of Br in the selective synthesis of thin-walled carbon-nanotubes with micrometre-length Fe3C-filling, Fe_3C tip-filled carbon nanotubes or empty carbon nanotubes by pyrolysis of ferrocene and (6-bromohexyl)ferrocene mixtures, Rsc Adv 5 (2015) 53956–53962.
[34] S.W. Pattinson, R.E. Diaz, N.A. Stelmashenko, A.H. Windle, C. Ducati, E.A. Stach, K.K.K. Koziol, In situ observation of the effect of nitrogen on carbon nanotube synthesis, Chem. Mater. 25 (2013) 2921–2923.
[35] K. Hata, D.N. Futaba, K. Mizuno, T. Namai, M. Yumura, S. Iijima, Water-assisted highly efficient synthesis of impurity-free single-walled carbon nanotubes, Science 306 (2004) 1362–1364.
[36] M. Jiang, C. Fu, R. Cheng, T. Liu, M. Guo, P. Meng, J. Zhang, B. Sun, Interface engineering of Co_3Fe_7-Fe_3C heterostructure as an efficient oxygen reduction reaction electrocatalyst for aluminum-air batteries, Chem Eng J 404 (2021) 127124.
[37] T.T. Zhao, A. Kumar, X.Y. Xiong, M. Ma, Y.Y. Wang, Y. Zhang, S. Agnoli, G.X. Zhang, X.M. Sun, Assisting atomic dispersion of Fe in N-doped carbon by aerosil for high-efficiency oxygen reduction, Acs Appl Mater Inter 12 (2020) 25832–25842.
[38] Z.-H.W. Kuan-Chieh Li, Chun-Hung Ke, Yao-Chang Lee, Jyh-Fu Lee, Jin-Ming Chen, Shu-Chih Haw, Fu-Te Tsai, Wen-Feng Liaw, Selectivity and activity modulation of electrocatalytic carbon dioxide reduction by atomically dispersed dual iron catalysts, J. Mater. Chem. A 11 (2023) 2377–2390.
[39] M.S. Ferrandon, J.H. Park, X.P. Wang, E. Coleman, A.J. Kropf, D.J. Myers, Enhancing the activity of Fe-N-C oxygen reduction reaction electrocatalysts by high-throughput exploration of synthesis parameters, Electrochim. Acta 441 (2023) 141850.
[40] H.W.K. Seok Ki Kim, Seung Ju Han, Sung Woo Lee, Jungho Shin, Yong Tae Kim, Mechanistic and microkinetic study of non-oxidative methane coupling on a single-atom iron catalyst, Commun. Chem. 3 (2020) 58.
[41] A. Zitolo, V. Goellner, V. Armel, M.T. Sougrati, T. Mineva, L. Stievano, E. Fonda, F. Jaouen, Identification of catalytic sites for oxygen reduction in iron- and nitrogen-doped graphene materials, Nat. Mater. 14 (2015) 937.
[42] J. Lin, Y.H. Du, G.P. Wu, C. Wang, L. Guo, Y.Z. Wang, Fe/N co-doped hierarchically porous carbon on N-doped carbon nanotubes towards oxygen reduction reaction, Int. J. Hydrogen Energy 48 (2023) 640–647.

[43] T. Huang, S. Mao, M. Qiu, O. Mao, C. Yuan, J. Chen, Nitrogen-boron dipolar-doped nanocarbon as a high-efficiency electrocatalyst for oxygen reduction reaction, Electrochim. Acta 222 (2016) 481–487.
[44] K.K. Li, Y.T. Zhang, P. Wang, X.Y. Long, L.S. Zheng, G.Y. Liu, X.F. He, J.S. Qiu, Core-Shell ZIF-67@ZIF-8-derived multi-dimensional cobalt-nitrogen doped hierarchical carbon nanomaterial for efficient oxygen reduction reaction, J Alloy Compd 903 (2022) 163701.
[45] K. Gong, F. Du, Z. Xia, M. Durstock, L. Dai, Nitrogen-doped carbon nanotube arrays with high electrocatalytic activity for oxygen reduction, Science 323 (2009) 760–764.
[46] Q.Q. Fan, J.N. Su, T. Sun, Z.H. Bi, H.S. Wang, S.S. Zhang, Q.J. Liu, L.Z. Zhang, G.Z. Hu, Advances of the functionalized carbon nitrides for electrocatalysis, Carbon Energy 4 (2022) 211–236.
[47] Y. Lu, X. Li, A. Kaliyaraj Selva Kumar, R.G. Compton, Does nitrogen doping enhance the electrocatalysis of the oxygen reduction reaction by multiwalled carbon nanotubes? ACS Catal. 12 (2022) 8740–8745.
[48] M.R. Wang, W.J. Yang, X.Z. Li, Y.S. Xu, L.R. Zheng, C.L. Su, B. Liu, Atomically dispersed Fe-heteroatom (N, S) bridge sites anchored on carbon nanosheets for promoting oxygen reduction reaction, ACS Energy Lett. 6 (2021) 379–386.
[49] A. Volperts, A. Plavniece, K. Kaare, G. Dobele, A. Zhurinsh, I. Kruusenberg, Influence of chemical activation temperatures on nitrogen-doped carbon material structure, pore size distribution and oxygen reduction reaction activity, Catalysts 11 (2021) 1460.
[50] H.Y. Zhu, M.X. Leng, X.B. Ge, X. Chen, Enhanced oxygen reduction reaction activity by utilizing carbon nanotube intramolecular junctions, Comput Theor Chem 1214 (2022) 113765.
[51] Y. Zhou, Y. Yu, D. Ma, A.C. Foucher, L. Xiong, J. Zhang, E.A. Stach, Q. Yue, Y. Kang, Atomic Fe dispersed hierarchical mesoporous Fe–N–C nanostructures for an efficient oxygen reduction reaction, ACS Catal. 11 (2020) 74–81.
[52] J. Liang, Y. Zheng, J. Chen, J. Liu, D. Hulicova-Jurcakova, M. Jaroniec, S.Z. Qiao, Facile oxygen reduction on a three-dimensionally ordered macroporous graphitic C_3N_4/carbon composite electrocatalyst, Angew Chem Int Edit 51 (2012) 3892–3896.
[53] Y. Zhang, Y.-y. Zhang, C.-e. Li, X.-h. Yan, S. Hu, R.-b. Yin, Y.-f. Wei, K.-z. Gao, H.-l. Gao, Research progress of $NiFe_2O_4$ electrode materials in supercapacitors: preparation, modification, structural regulation, and future challenges, Coordin Chem Rev 519 (2024) 216103.
[54] T.H. Hengyi Fang, Dong Liang, Ming Qiu, Yue Sun, Shuo Yao, Yu Jiemei, M. Mayilvel Dinesh, Zhongqin Guo, Ying Xia, Shun Mao, Prussian blue analog-derived 2D ultrathin $CoFe_2O_4$ nanosheets as high-activity electrocatalysts for oxygen evolution reaction in Aakaline and neutral mediums, J. Mater. Chem. A 7 (2019) 7328–7332.
[55] S. Wang, D. Yu, L. Dai, D.W. Chang, J.-B. Baek, Polyelectrolyte-functionalized graphene as metal-free electrocatalysts for oxygen reduction, ACS Nano 5 (2011) 6202–6209.
[56] B. Wang, K. Srinivas, Y. Liu, D. Liu, X. Zhang, W. Zhang, Y. Chen, N-doped CNTs capped with carbon layer armored CoFe alloy as highly stable bifunctional catalyst for oxygen electrocatalysis, Nano Res. 15 (2022) 3971–3979.
[57] B.F. Gao, M.Y. Tan, W.H. Xi, X.F. Lin, Z.N. Li, M.R. Shen, B.Z. Lin, Co-embedded carbon nanotubes modified N-doped carbon derived from poly(Schiff base) and zeolitic imidazole frameworks as efficient oxygen electrocatalyst towards rechargeable Zn-air battery, J. Power Sources 527 (2022) 231205.
[58] M. He, R. Li, C. Cheng, C. Liu, B. Zhang, Microenvironment regulation breaks the Faradaic efficiency-current density trade-off for electrocatalytic deuteration using $D_{(2)}O$, Nat. Commun. 15 (2024) 5231.
[59] Y. Zhang, C.-g. Zhou, X.-h. Yan, Y. Cao, H.-l. Gao, H.-w. Luo, K.-z. Gao, S.-c. Xue, X. Jing, Recent advances and perspectives on graphene-based gels for superior flexible all-solid-state supercapacitors, J. Power Sources 565 (2023) 232916.